PNAS
www.pnas.org

Supplementary Information for

Regulation and Drug Modulation of a Voltage-Gated Sodium Channel: Pivotal Role of the S4-S5 Linker in Activation and Slow Inactivation

Jinglei Xiao, Vasyl Bondarenko, Yali Wang, Antonio Suma, Marta Wells, Qiang Chen, Tommy Tillman, Yan Luo, Buwei Yu, William P. Dailey, Roderic Eckenhoff, Pei Tang, Vincenzo Carnevale, Michael L. Klein, Yan Xu

Corresponding authors: Professor Yan Xu or Professor Michael L. Klein
Email: xu2@pitt.edu or mlklein@temple.edu

This PDF file includes:

Experimental Details

Heterologous Expression of NaChBac

The same expression system as detailed previously (1) was used. Point mutations were introduced into the WT NaChBac cDNA in a modified pLenti6-CMV2 expression vector using the QuikChange site-directed mutagenesis method (Agilent). cDNA was amplified in New England Biolabs (Ipswich, MA) stable competent *E. coli* (NEB C3040). HEK-293 cells transiently transfected using polyethylenimine (Polysciences, Warrington, PA) transfection protocol were cultured in Dulbecco's modified Eagle's medium/F-12 (Invitrogen, Carlsbad, CA) with 5% (v/v) fetal bovine serum (BioSource International, Camarillo, CA) and 5%/95% CO_2/O_2 (v/v) at 37°C for 24-48 hours before electrophysiology recording.

Electrophysiology

Whole-cell patch clamping experiments were performed using an IonFlux Mercury HT automated electrophysiology instrument (Fluxion Biosciences, Alameda, CA), which allows groups of up to 64 independent measurements to be collected simultaneously, with each individual measurement consisting of averaged responses from 20 parallel cells. The extracellular solution (ECS) contained (in mM): 140 NaCl, 4 KCl, 1.5 $CaCl_2$, 1.5 $MgCl_2$, 10 Hepes, 5 D-glucose, and pH 7.4 adjusted using NaOH. The intracellular solution (ICS) contained (in mM): 15 NaCl, 80 CsF, 40 CsCl, 10 EGTA, 10 Hepes, and pH 7.3 adjusted with CsOH. The measured osmolality for ECS and ICS was 310 and 295 mOsm/kg H_2O, respectively. A 200-mM stock solution of propofol or 4fp was dissolved in DMSO and then diluted to experimental concentrations by ECS. CBFS was purchased as sodium salt (Sigma-Aldrich Inc, St. Louis, MO). The stock solution of CBFS (200 μM) was prepared in DMSO and diluted by ECS to the desired concentrations. All dilutions were prepared to have a final concentration of 0.05% DMSO and used on the same day. In all experiments, control recordings were collected prior to the additions of the anesthetic or CBFS conjugation. Following the baseline recordings, 1 μM propofol or 4fp was perfused for 2 minutes before data collection. For CBFS conjugation, 10 μM CBFS was perfused for 30 s, followed by 2 minutes wash with ECS, before additional measurements with and without exposure to propofol (or 4fp) were conducted.

The standard protocol for voltage-dependent activation of Na^+ currents consisted of 200-ms depolarizing steps in increments of ΔV = 10 mV from –100 to +60 mV. The holding potential (V_{hold}) was –100 mV. In mutants that showed no activation in this voltage range, measurements were repeated with depolarization steps from –100 to +290 mV in 15-mV increments. Pre-pulse inactivation was assessed with a two-pulse protocol: (1) a 2-s conditioning pulse in increments of ΔV = 10 mV from –120 mV to 0 mV, followed immediately by (2) a 50-ms test pulse to –20 mV (V_{hold} = –100 mV). The peak chord conductance (G) was calculated by

$$G = \frac{I}{(V - V_{rev})} \quad (1)$$

where I is the peak Na^+ current, V is the test potential, and V_{rev} is the Na^+ reversal potential. G was normalized to the maximum peak conductance G_{max} and voltage dependence of activation (G-V curve) was fit to Boltzmann function:

$$G(V) = \frac{G_{max}}{\left[1 + e^{\frac{V_{\frac{1}{2}a} - V}{k_a}}\right]} \quad (2)$$

where $V_{1/2a}$ is the midpoint voltage of activation and k_a is the slope factor. Similarly, the pre-pulse inactivation parameters were fit to Boltzmann function:

$$I(V) = \frac{I_{max}}{\left[1+e^{\frac{V_{\frac{1}{2}in}-V}{k_{in}}}\right]} \quad (3)$$

where I_{max} is the maximum current amplitude, $V_{1/2in}$ is the midpoint voltage of inactivation, and k_{in} is the slope factor. Time constants of activation (τ_a) and inactivation (τ_{in}) were derived from the rising and decaying components of the Na^+ current, respectively, by fitting to single exponential function

$$I(t) = \left(Ae^{\pm\frac{t}{\tau}} + C\right) \quad (4)$$

where A is the amplitude, C is the plateau constant, t is time, and τ is the time constant of activation or inactivation.

NMR data acquisition and analysis

The same procedures as described previously were used for cysteine mutations and ^{19}F labeling with BTFA (1, 2). Briefly, purified NaChBac with a single-point cysteine mutation was treated briefly with the reducing agent tris-(2-carboxyethyl)phosphine (TCEP). After removing TCEP on a desalting column, BTFA in 50x molar access was incubated with the protein for 3 hours at room temperature and then overnight at 4°C. Free ^{19}F labels were removed by 3 exchanges of dialysis in 100x volume, followed by size exclusion chromatography. Typical NMR samples contain ~100 μM NaChBac in 1-2% n-dodecyl-β-D-maltose (DDM), 100 mM NaCl, 50 mM Tris at pH 7.7, and 5% D_2O for frequency lock. Typically, 4fp was titrated into NMR samples up to 200 μM for STD measurements. All NMR spectra were acquired at 10°C using a ^{19}F-cryoprobe on a Brucker Biospin Avance 600 spectrometer.

The STD NMR spectra were derived from interleaving collections of on- and off-resonance ^{19}F spectra with frequency-selective saturations at −83.8 and −45.00 ppm, respectively. Selective saturation of different durations, ranging from 0.05 s to 4.0 s, was achieved by a train of 3-ms Gaussian-cascade-(Q3.1000)-shaped pulses spaced by inter-pulse delays of 3-ms each. The intensities and corresponding errors of 4fp ^{19}F peak were analyzed using Mnova and TopSpin. Graphpad Prism software was used to fit the STD data to the mono-exponential function:

$$STD = STD_{max}(1 - e^{-k_{sat}t}) \quad (5)$$

where t is the saturation time, STD_{max} is the maximum (plateau) STD, k_{sat} is the saturation rate constant, and STD is calculated from the 4fp spectral intensities with on- and off-resonance saturation of the protein peak, I_{on} and I_{off}, respectively:

$$STD = \frac{I_{off}-I_{on}}{I_{off}} \times 100 \quad (6)$$

The site-selective binding of the ligand at the ^{19}F-labeled site is measured by the cross-relaxation rate constant, σ:

$$\sigma = STD_{max} \times k_{sat} \quad (7)$$

Molecular dynamics simulations

Experimental NaChBac structures were not available until recently when cryo-EM structures in inactivated states were reported (3). To gain insights into the structural basis of functional changes, we modeled the resting, activated (open), and inactivated (closed) structures of NaChBac by comparing several experimental structures of prokaryotic and eukaryotic Na_V channels as templates. Specifically, we referenced PDB ID 6P6W of NavAb for the resting state (4), 5HVX of NavMs (5), 6A90 of NavPas (6), and 5XSY/6AGF of Nav1.4 (7, 8) for various structural features of an open conformation, as well as 5VB2 of NavAb (9) for inactivated states. The homology models were built using SWISS-MODEL software (10). Refinement of sidechain rotameric states was performed using the software Scwrl (11). The modeled inactivated structures were not significantly different from the recently published cryo-EM structures (6VX3/6VWX) of NaChBac (3): the root-mean-squared deviation (RMSD) between the homology model of the closed state (initial frame of our simulation) and the NaChBac cryoEM model (pdb code: 6VWX) is 2.5 Å (considering all non-hydrogen atoms) and 1.6 Å (considering only the backbone atoms). Importantly, the cryo-EM structures of an inactivated NaChBac show the interaction between T140 of the S4-S5 linkers and N225 of the domain-swapped S6 helices.

The molecular systems for MD simulations were assembled using CHARMM-GUI (12) and the channel models were embedded in a fully hydrated POPC lipid bilayer. The number of ions in the bulk was set to 0.15 M KCl. Each molecular system contained about 180,000 atoms. Calculations were performed using the NAMD 2.12 software (13), using the all-atom potential energy function CHARMM36 for protein and phospholipids and the TIP3P potential for water molecules (14, 15). Periodic boundary conditions were applied, and long-range electrostatic interactions were treated by the particle mesh Ewald algorithm (16). The 4-fluoropropofol molecule (4fp) was modeled using the CGenFF webserver (17, 18). Molecular systems were equilibrated for 2 ns with decreasing harmonic restraints on the protein atoms, the pore ions, and the water molecules localized in the selectivity filter. Restraints were removed in the production run. To model four 4fp molecules bound to the closed conformation, we considered the final configuration of our previous flooding simulation with propofol; the propofol molecules bound to the four equivalent T140 pockets were chemically modified into 4fp and subject to energy minimization. All trajectories were generated with a time step of 2 fs at constant normal pressure (1 atm) controlled by a Langevin piston and constant temperature (300 K) using a Nosé-Hoover thermostat. Pore radius profiles were calculated using the HOLE software (19).

Statistical analyses were performed using Prism 8.1.2 (GraphPad Software, San Diego, CA). All evaluated parameters in electrophysiology were reported as mean ± SEM. The paired-samples t-test was used to assess significant differences between paired sets from the same cells in the absence and presence of propofol and/or CBFS. A p value of 0.05 was considered significant.

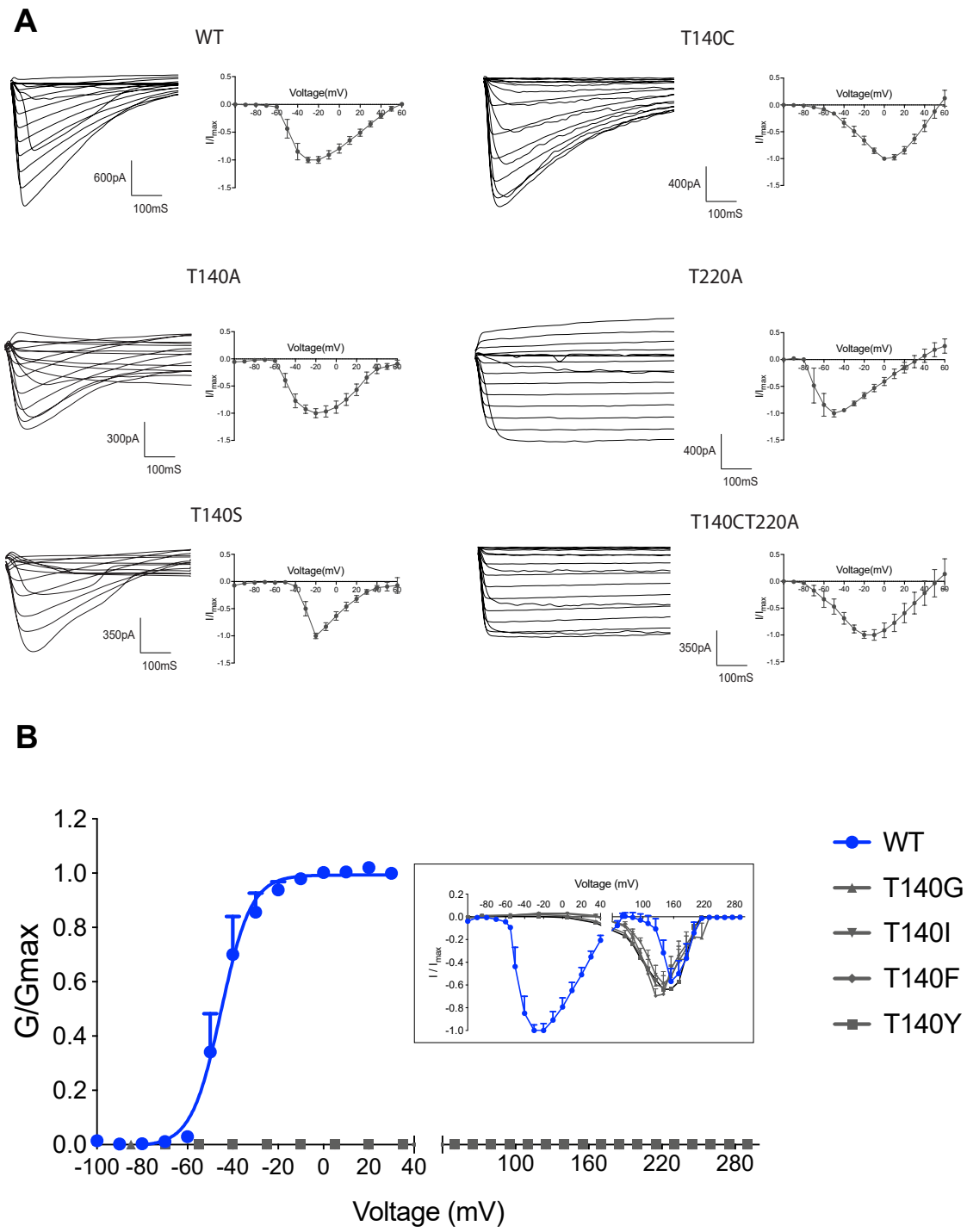

Fig. S1. (**A**) Electrophysiology measurements of WT NaChBac and various mutants showing voltage-dependent activations in T140A, T140S, T140C, and the inactivation-disabled mutants T220A and T140C/T220A. (**B**) Mutations at T140 with side chains too small or too large compared to Thr are non-functional with activation voltages ranging from –100 mV to +290 mV. Data are shown as mean ± SEM from n = 7-15 independent measurements.

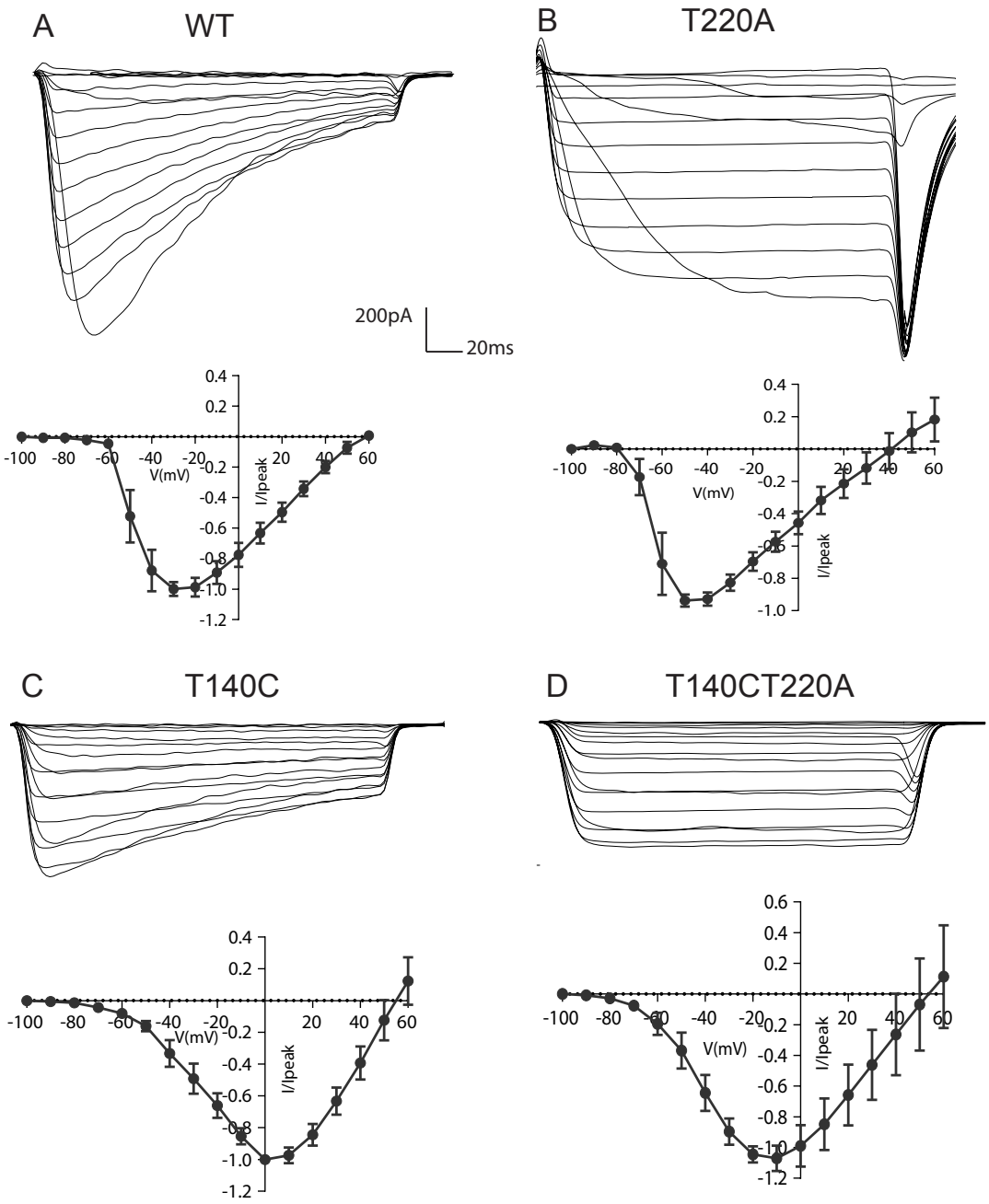

Fig. S2. Mutation-induced abolition of slow inactivation. (**A**) Representative traces of voltage-dependent activation in the WT NaChBac, along with the averaged I-V curves from multiple independent measurements. (**B**) The single-point mutation T220A is known to abolish slow inactivation of NaChBac. This mutation prepositions the channel in an activated state, as reflected in the large left shift of the I-V curve. (**C** and **D**) The same T220A mutation introduced into the T140C channel produced the same elimination of slow inactivation. The T140C and T140C/T220A constructs allowed for ^{19}F labeling at the Cys residue in T140C to measure site-specific binding by NMR in activated and inactivated conformations. Data are shown as mean ± SEM (n > 7).

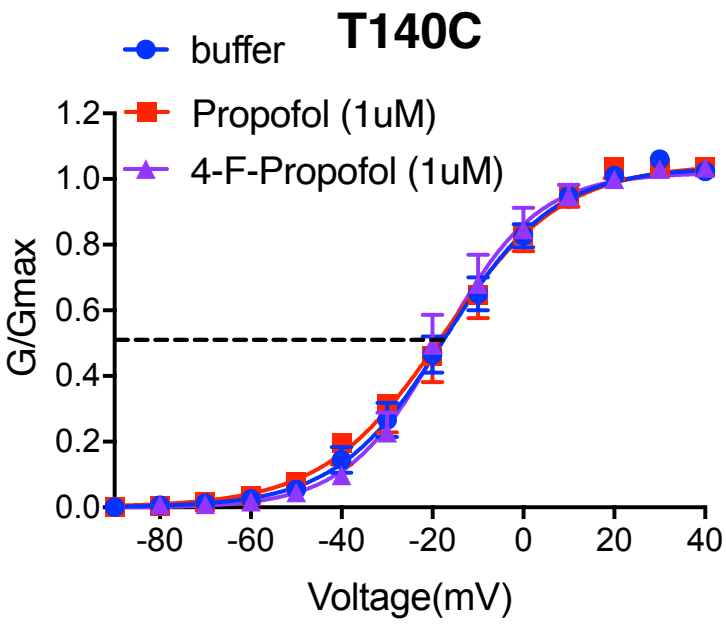

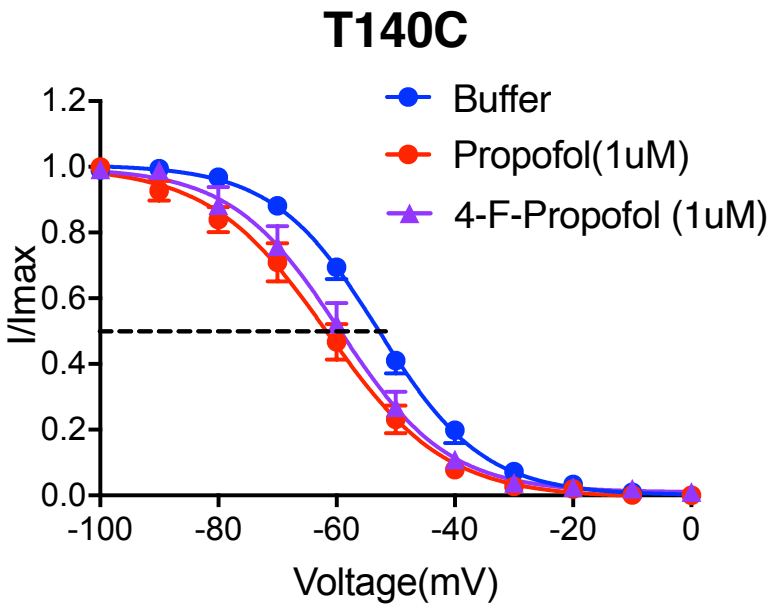

Fig. S3. Nearly identical effects of propofol and 4fp on activation and slow inactivation of T140C NaChBac. In addition to the similar functional effects on the WT NaChBac and the same anesthetizing concentrations between propofol and 4fp, the comparable results of propofol and 4fp on T140C, as shown here, validate the use of 4fp as a molecular probe in the ^{19}F-NMR STD measurements of the specific propofol binding at the T140 site. Values are given as mean ± SEM (n = 7-10).

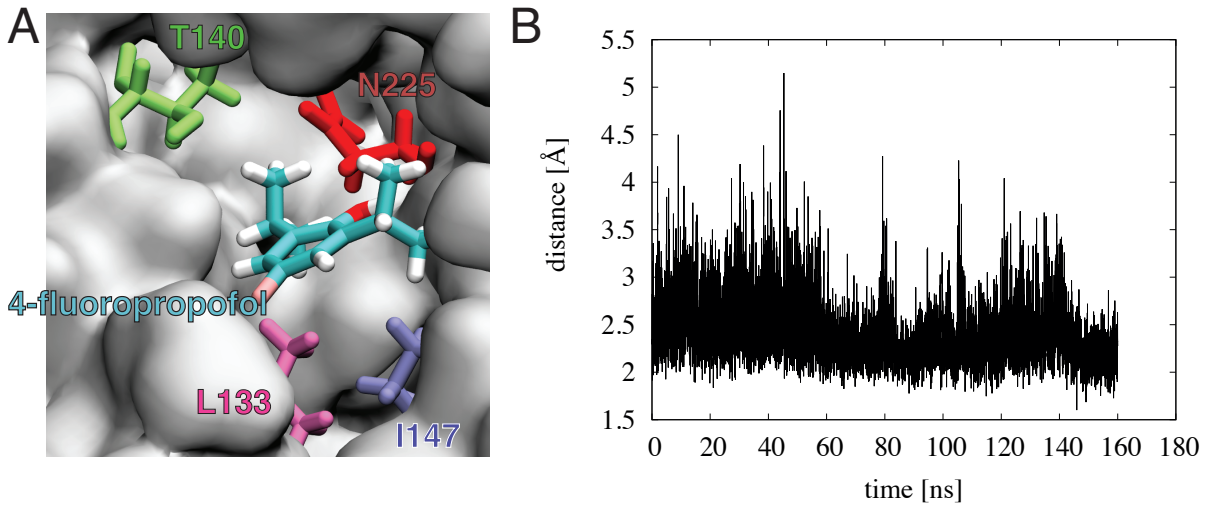

Fig. S4. 4-fluoropropofol (4fp) binding in pocket between the S4-S5 linker and S6 helices. (**A**) A typical pose of 4fp within the pocket near T140 in the S4-S5 linker from molecular dynamics simulations. The orientations of 4fp and the binding pocket marked by residues L133 (pink) and T140 (green) in the S4-S5 linker and I147 (purple) and N225 (red) from the adjacent subunit are shown as sticks. (**B**) The time dependence of the minimum among all-atom distances between 4fp and L133/I147 atoms at the distal end of the T140 pocket in the closed, inactivated structure model. 4fp is consistently bound to the T140 pocket throughout the entire 160 ns simulations.

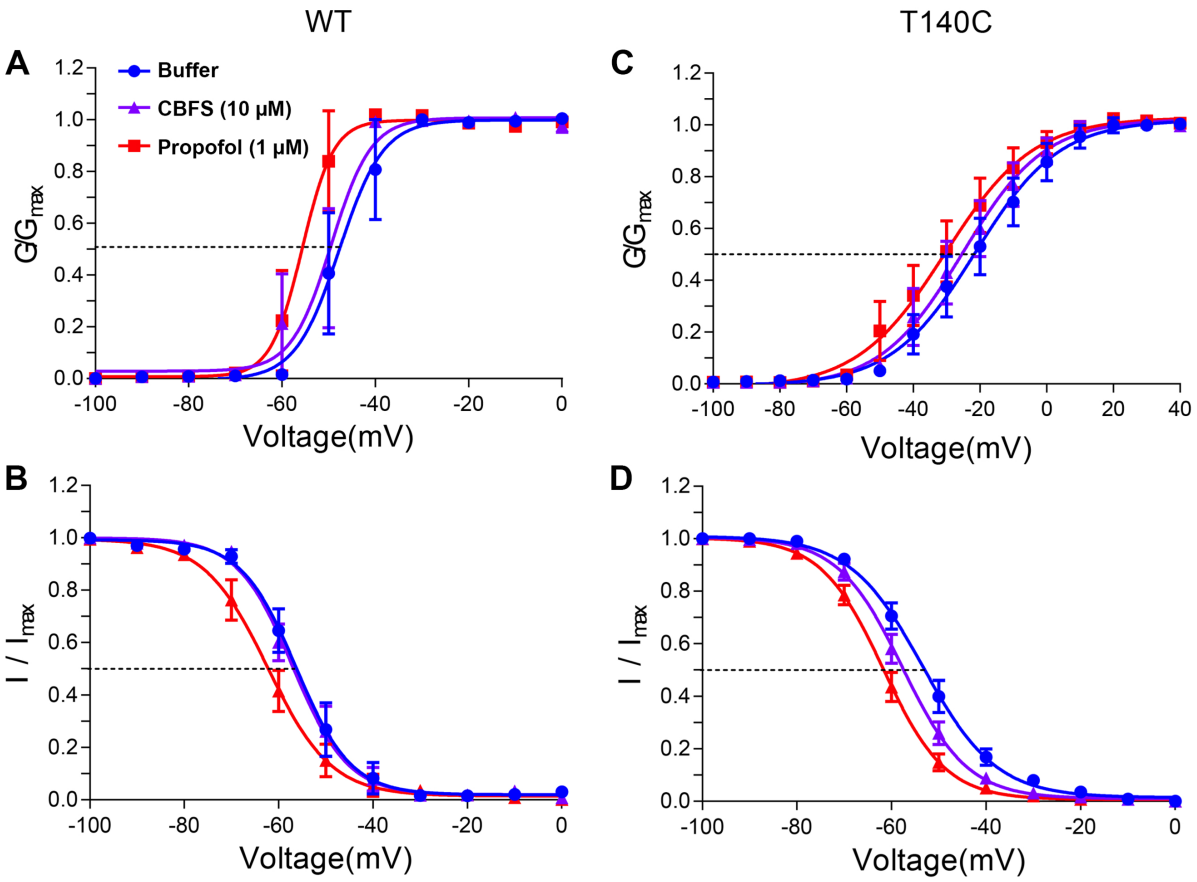

Fig. S5. Effects of covalent modification of the T140 binding pocket on channel gating and propofol binding. Steady-state activation (**A** and **C**) and inactivation (**B** and **D**) of the WT and T140C NaChBac, respectively, before (blue) and after (purple) conjugation reaction with 8-(chloromercuri)-2-dibenzofuransulfonic acid (CBFS), followed by exposure to 1 μM propofol (red) after washout of CBFS. Conjugation can only occur at the cysteine side chain in T140C since no other cysteine residues are naturally present in NaChBac. Data are presented as mean ± SEM (n = 6-8) and solid lines are best fit to the data using Eq. (2) or Eq. (3) with the CBFS- and propofol-induced changes summarized in Table S4.

Table S1. Baseline gating parameters of NaChBac WT and mutants[†]

Parameters	WT	T140A	T140S	T140C	T220A	T140C/T220A
$V_{1/2a}$	–45.7±0.82	–33.6±1.61**	–30.4±0.52***	–25.8±1.51***	–64.7±1.13**	–34.6±1.14**
k_a	5.5 ±0.69	10.1±1.43*	3.9±0.57	11.0±1.36**	5.4±0.91	10.9±0.99*
$V_{1/2in}$	–52.4±1.30	–52.8±1.07	–48.4±1.41	–54.3±0.77	/	/
k_{in}	7.1±1.15	8.3±0.95	7.87±1.24	9.1±0.69*	/	/

[†]Values are given as mean ± SEM (n = 6-11). Gating parameters of NaChBac WT and mutant are evaluated by unpaired t test: * $p < 0.05$, ** $p < 0.01$, *** $p < 0.001$.

Table S2. Propofol-induced changes in gating parameters of NaChBac WT and mutants[†]

Parameters	WT	T140A	T140S	T140C
$\Delta V_{1/2a}$	–9.3 ±2.9***	–0.74±1.6	–10.0±2.3*	–2.4±0.8*
$\Delta V_{1/2in}$	–7.3 ±2.5**	–0.5±1.8	–3.5±2.9	–7.8±2.2*

[†]Values are given as mean ± SEM (n = 5-10). Gating parameters of NaChBac WT and mutant are evaluated by paired t test: * $p < 0.05$, ** $p < 0.01$, *** $p < 0.001$.

Table S3. **Comparison of fitting parameters of ^{19}F-NMR STD in 4-fluoropropofol**

^{19}F-Labeled Mutant	STD_{max} (%)	k_{sat} (s^{-1})	σ×100 (s^{-1})
T140C	18.1±1.4	1.7±0.4	30.9±7.8
T140C/T220A	~2% (@2s)	/	/
F227C	17.4±0.9	2.5±0.4	42.6±7.6
F227C/T220A	17.2±1.1	1.6±0.3	27.5±5.4

Table S4. Effect of CBFS and propofol on gating parameter changes in NaChBac[†]

Drugs	Parameters	WT	T140C	T220A	T140C/T220A
Propofol	$\Delta V_{1/2a}$	–9.3 ±2.9***	–2.4±0.8*	–7.9±1.9*	6.1±1.7*
	$\Delta V_{1/2in}$	–7.3 ±2.5**	–7.8±2.2*	/	/
CBFS	$\Delta V_{1/2a}$	–1.2 ±0.7	–4.3±0.9**	–2.0±1.0	–6.9±0.9**
	$\Delta V_{1/2in}$	–0.3 ±1.0	–4.5±0.9**	/	/
CBFS+ Propofol	$\Delta V_{1/2a}$	–6.6±1.4**	–4.6±1.8**	–8.4±1.4**	3.5±1.3*
	$\Delta V_{1/2in}$	–5.5±1.2**	–4.0±0.8**	/	/

[†]Values are reported as mean ± SEM (n = 6-8). Gating parameters of NaChBac WT and mutants evaluated by paired t test: * $p < 0.05$, ** $p < 0.01$, *** $p < 0.001$.

References

1. Wang YL, Yang E, Wells MM, Bondarenko V, Woll K, Carnevale V, et al. Propofol inhibits the voltage-gated sodium channel NaChBac at multiple sites. J Gen Physiol. 2018;150(9):1317-31.
2. Bondarenko V, Wells MM, Chen Q, Singewald KC, Saxena S, Xu Y, et al. ^{19}F Paramagnetic Relaxation-Based NMR for Quaternary Structural Restraints of Ion Channels. ACS chemical biology. 2019;14(10):2160-5.
3. Gao S, Valinsky WC, On NC, Houlihan PR, Qu Q, Liu L, et al. Employing NaChBac for cryo-EM analysis of toxin action on voltage-gated Na(+) channels in nanodisc. Proceedings of the National Academy of Sciences of the United States of America. 2020;117(25):14187-93.
4. Wisedchaisri G, Tonggu L, McCord E, Gamal El-Din TM, Wang L, Zheng N, et al. Resting-State Structure and Gating Mechanism of a Voltage-Gated Sodium Channel. Cell. 2019;178(4):993-1003 e12.
5. Sula A, Booker J, Ng LCT, Naylor CE, DeCaen PG, Wallace BA. The complete structure of an activated open sodium channel. Nature communications. 2017;8.
6. Shen HZ, Li ZQ, Jiang Y, Pan XJ, Wu JP, Cristofori-Armstrong B, et al. Structural basis for the modulation of voltage-gated sodium channels by animal toxins. Science. 2018;362(6412).
7. Pan X, Li Z, Zhou Q, Shen H, Wu K, Huang X, et al. Structure of the human voltage-gated sodium channel Nav1.4 in complex with beta1. Science. 2018;362(6412).
8. Yan Z, Zhou Q, Wang L, Wu J, Zhao Y, Huang G, et al. Structure of the Nav1.4-beta1 Complex from Electric Eel. Cell. 2017;170(3):470-82 e11.
9. Lenaeus MJ, El-Din TMG, Ing C, Ramanadane K, Pomes R, Zheng N, et al. Structures of closed and open states of a voltage-gated sodium channel. Proceedings of the National Academy of Sciences of the United States of America. 2017;114(15):E3051-E60.
10. Waterhouse A, Bertoni M, Bienert S, Studer G, Tauriello G, Gumienny R, et al. SWISS-MODEL: homology modelling of protein structures and complexes. Nucleic acids research. 2018;46(W1):W296-W303.
11. Krivov GG, Shapovalov MV, Dunbrack RL, Jr. Improved prediction of protein side-chain conformations with SCWRL4. Proteins. 2009;77(4):778-95.
12. Wu EL, Cheng X, Jo S, Rui H, Song KC, Davila-Contreras EM, et al. CHARMM-GUI Membrane Builder toward realistic biological membrane simulations. J Comput Chem. 2014;35(27):1997-2004.
13. Phillips JC, Braun R, Wang W, Gumbart J, Tajkhorshid E, Villa E, et al. Scalable molecular dynamics with NAMD. J Comput Chem. 2005;26(16):1781-802.
14. Mackerell AD, Jr., Feig M, Brooks CL, 3rd. Extending the treatment of backbone energetics in protein force fields: limitations of gas-phase quantum mechanics in reproducing protein conformational distributions in molecular dynamics simulations. J Comput Chem. 2004;25(11):1400-15.
15. Jorgensen WL, Chandrasekhar J, Madura JD, Impey RW, Klein ML. Comparison of Simple Potential Functions for Simulating Liquid Water. J Chem Phys. 1983;79(2):926-35.
16. Essmann U, Perera L, Berkowitz ML, Darden T, Lee H, Pedersen LG. A Smooth Particle Mesh Ewald Method. J Chem Phys. 1995;103(19):8577-93.
17. Vanommeslaeghe K, MacKerell AD, Jr. Automation of the CHARMM General Force Field (CGenFF) I: bond perception and atom typing. Journal of chemical information and modeling. 2012;52(12):3144-54.
18. Vanommeslaeghe K, Raman EP, MacKerell AD, Jr. Automation of the CHARMM General Force Field (CGenFF) II: assignment of bonded parameters and partial atomic charges. Journal of chemical information and modeling. 2012;52(12):3155-68.

19. Smart OS, Neduvelil JG, Wang X, Wallace BA, Sansom MS. HOLE: a program for the analysis of the pore dimensions of ion channel structural models. Journal of molecular graphics. 1996;14(6):354-60, 76.